

Hydroquinone and Quinone-grafted Porous Activated Carbons for Highly Selective CO₂ Capture from Flue Gases and Natural Gas Upgrading

Jun Wang ^a, Rajamani Krishna ^b, Jiangfeng Yang ^c, Shugaung Deng ^{a*}

^a. Chemical Engineering Department,
New Mexico State University,
Las Cruces, New Mexico, 88003, USA

^b. Van't Hoff Institute for Molecular Sciences,
University of Amsterdam,
Science Park 904, 1098 XH Amsterdam, The Netherlands

^c. Research Institute of Special Chemicals,
Taiyuan University of Technology,
Taiyuan 030024, Shanxi, PR China

*Corresponding author: Tel: +1-575-646-4346; Fax: +1-575-646-7706.

-E-mail address: sdeng@nmsu.edu

Table of Contents

1. Figure S1. XRD patterns of OACs.....	3
2. Figure S2. Representative SEM images of the a) OAC-1, b) OAC-1 and c) OAC-2 showing the similarity in the pore structure of the carbon pre- and post-modification.....	3
3. Figure S3. CO ₂ adsorption 323K of OAC-0, OAC-1, and OAC-2.	4
4. Figure S4. (a) CH ₄ and N ₂ adsorption 323K of OAC-0, OAC-1, and OAC-2.	4
5. Fitting of pure component isotherms.....	5
6. Table S1. 1-site Langmuir parameters for adsorption of CO ₂ in different OACs.	5
7. Table S2. 1-site Langmuir parameters for CH ₄ in different OACs.....	6
8. Table S3. 1-site Langmuir parameters for N ₂ in different OACs.....	6
9. IAST calculations.....	7
10. Isosteric heat of adsorption.....	7
11. Table S4. Isosteric heats of adsorption of CO ₂ , CH ₄ and N ₂ in different OACs.....	8
12. Figure S5. CO ₂ , CH ₄ , and N ₂ fractional uptake on (a) OAC-1, (b) OAC-2 at 323 K.....	8
13. Table S5. Summary of Diffusion Time Constants of CO ₂ , CH ₄ , and N ₂ on the OACs at 323 K.....	9
14. Simulation methodology for transient breakthrough in fixed bed adsorbers	9
15. Figure S6. Schematic of the breakthrough apparatus.....	13
16. Notation.....	14
17. Reference.....	15

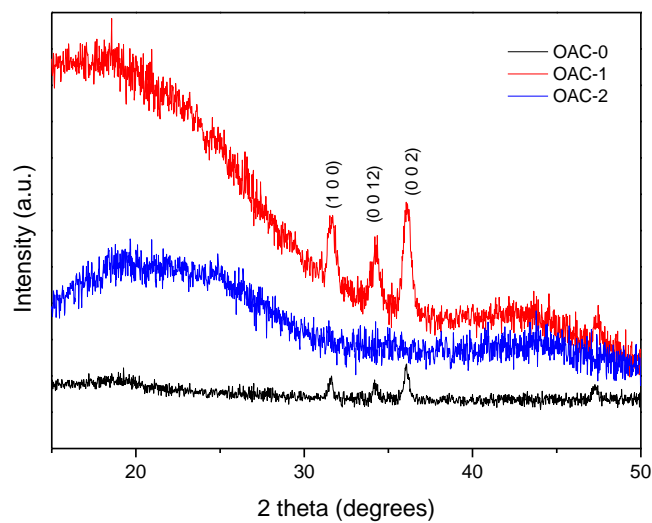


Figure S1. XRD patterns of OAC-1, OAC-1 and OAC-2.

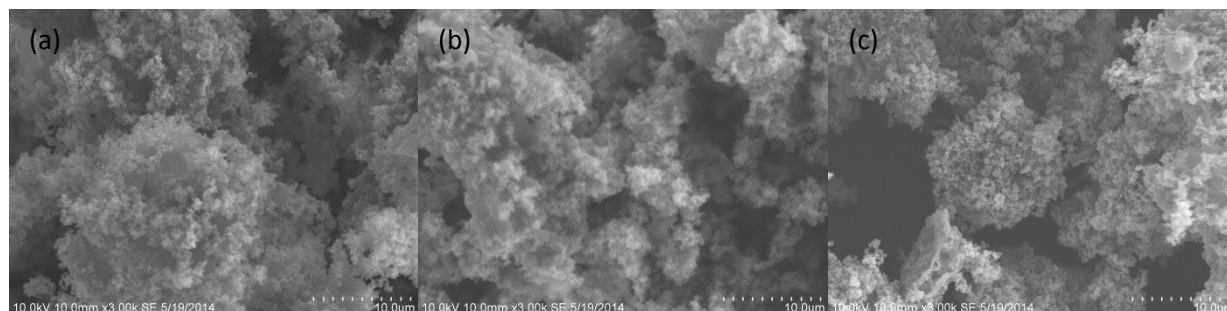


Figure S2. Representative SEM images of the a) OAC-1, b) OAC-1 and c) OAC-2 showing the similarity in the pore structure of the carbon pre- and post-modification.

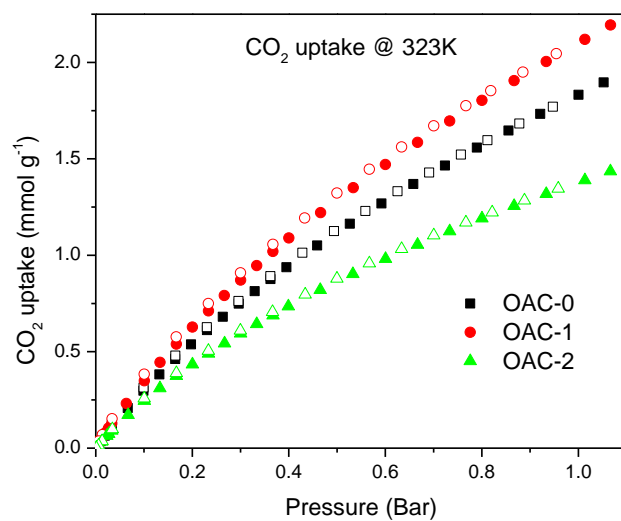


Figure S3. CO₂ adsorption 323K of OAC-0, OAC-1, and OAC-2.

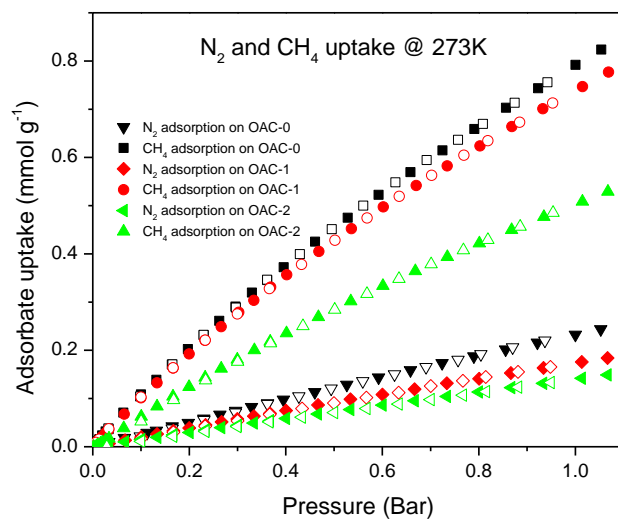


Figure S4. (a) CH₄ and N₂ adsorption 323K of OAC-0, OAC-1, and OAC-2.

Fitting of pure component isotherms

The experimentally measured loadings for (a) CO₂, (b) CH₄, and (c) N₂ were measured as a function of the absolute pressure at three different temperatures 273 K, 298 K, and 323 K.

The isotherm data for all three guest molecules in OAC-0, OAC-1, and OAC-2 were fitted with the Langmuir model

$$q = q_{sat} \frac{bp}{1 + bp} \quad (1)$$

with T -dependent parameter b

$$b = b_0 \exp\left(\frac{E}{RT}\right) \quad (2)$$

The Langmuir fit parameters are provided in Table S1, Table S2, and Table S3.

Table S5. 1-site Langmuir parameters for adsorption of CO₂ in different OACs.

	q_{sat} mol kg ⁻¹	b_0 Pa ⁻¹	E kJ mol ⁻¹
OAC-0	6.7	5.5×10^{-10}	23.8
OAC-1	7.6	6.34×10^{-10}	23.5
OAC-2	4.8	8.16×10^{-10}	23

Table S6. 1-site Langmuir parameters for CH₄ in different OACs.

	q_{sat} mol kg ⁻¹	b_0 Pa ⁻¹	E kJ mol ⁻¹
OAC-0	3.75	1.67×10^{-9}	19.8
OAC-1	3	2.11×10^{-9}	20
OAC-2	2.5	1.802×10^{-9}	20.9

Table S7. 1-site Langmuir parameters for N₂ in different OACs.

	q_{sat} mol kg ⁻¹	b_0 Pa ⁻¹	E kJ mol ⁻¹
OAC-0	3.1	2.08×10^{-9}	16
OAC-1	2.9	4.18×10^{-10}	19.6
OAC-2	2.3	6.65×10^{-10}	18.4

IAST calculations

The adsorption selectivity for the mixtures CH₄/N₂ and CO₂/CH₄ defined by

$$S_{ads} = \frac{q_1/q_2}{p_1/p_2}$$

were calculated according to IAST model proposed by Myers [1,2]. In above equation, q_1 and q_2 are the absolute component loadings of the adsorbed phase in the mixture. These component loadings are also termed the uptake capacities.

Isosteric heat of adsorption

The isosteric heat of adsorption, Q_{st} , defined as

$$Q_{st} = RT^2 \left(\frac{\partial \ln p}{\partial T} \right)_q$$

were determined using the pure component isotherm fits using the Clausius-Clapeyron equation, where Q_{st} (kJ/mol) is the isosteric heat of adsorption, T (K) is the temperature, p (kPa) is the pressure, R is the gas constant. The values of Q_{st} for CO₂, CH₄, and N₂ are provided in Table S4 of OACs.

Table S8. Isothermic heats of adsorption of CO₂, CH₄ and N₂ in different OACs.

	Q_{st, CO_2} kJ mol ⁻¹	Q_{st, CH_4} kJ mol ⁻¹	Q_{st, N_2} kJ mol ⁻¹
OAC-0	23.8	19.8	16
OAC-1	23.5	20	19.6
OAC-2	23	20.9	18.4

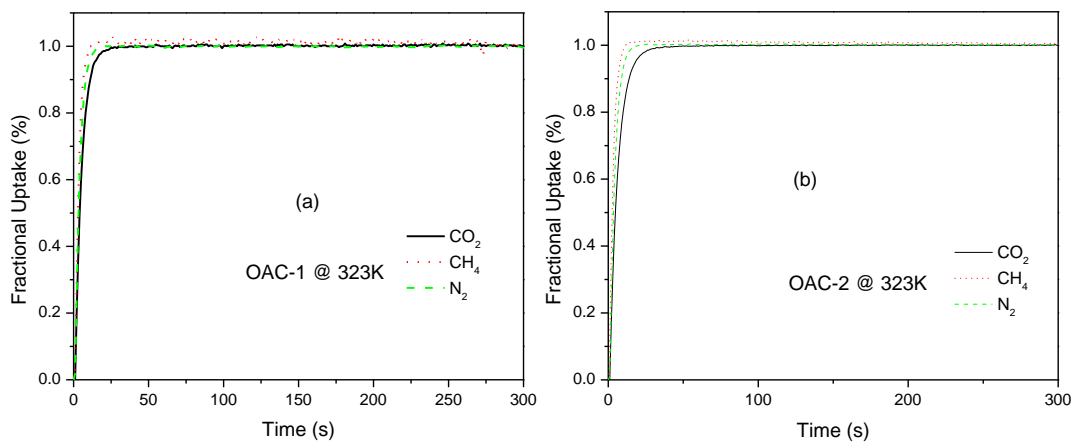


Figure S5. CO₂, CH₄, and N₂ fractional uptake on (a) OAC-1, (b) OAC-2 at 323 K.

Table S5. Summary of Diffusion Time Constants of CO₂, CH₄, and N₂ on the OACs at 323 K.

Sample	CO ₂ D_c/r_c^2 (10 ⁻³ s ⁻¹)	CH ₄ D_c/r_c^2 (10 ⁻² s ⁻¹)	N ₂ D_c/r_c^2 (10 ⁻³ s ⁻¹)
OAC-1	7.5	1.9	8.1
OAC-2	8.2	1.1	7.4

Simulation methodology for transient breakthrough in fixed bed adsorbers

The separation of CO₂/CH₄, CO₂/N₂, and CH₄/N₂ mixtures is commonly carried out in fixed bed adsorbers in which the separation performance is dictated by a combination of three separate factors: (a) adsorption selectivity, (b) uptake capacity, and (c) intra-crystalline diffusivities of guest molecules within the pores. Transient breakthrough simulations are required for a proper evaluation of microporous materials; the simulation methodology used in our work is described in earlier publications [3,4].

In order to evaluate the different OACs, breakthrough calculations were performed taking the following parameter values: inside diameter of tube = 50 mm; bed length, $L = 1.8$ m; voidage of bed, $\varepsilon = 0.5$; superficial gas velocity, $u = 0.05$ m/s (at inlet), interstitial velocity, $v = 0.1$ m/s. The mass of adsorbent packed in the tube is 2 kg; see schematic in Figure S6.

A brief summary of the simulation methodology is presented below. Assuming plug flow of an n -component gas mixture through a fixed bed maintained under isothermal conditions (see schematic in Figure 0), the partial pressures in the gas phase at any position and instant of time are obtained by solving the following set of partial differential equations for each of the species i in the gas mixture [5].

$$\frac{1}{RT} \frac{\partial p_i(t, z)}{\partial t} = -\frac{1}{RT} \frac{\partial (v(t, z) p_i(t, z))}{\partial z} - \frac{(1-\varepsilon)}{\varepsilon} \rho \frac{\partial \bar{q}_i(t, z)}{\partial t}; \quad i = 1, 2, \dots, n \quad (1)$$

In equation (1), t is the time, z is the distance along the adsorber, ρ is the framework density, ε is the bed voidage, v is the interstitial gas velocity, and $\bar{q}_i(t, z)$ is the *spatially averaged* molar loading within the crystallites of radius r_c , monitored at position z , and at time t .

At any time t , during the transient approach to thermodynamic equilibrium, the spatially averaged molar loading within the crystallite r_c is obtained by integration of the radial loading profile

$$\bar{q}_i(t) = \frac{3}{r_c^3} \int_0^{r_c} q_i(r, t) r^2 dr \quad (2)$$

For transient unary uptake within a crystal at any position and time with the fixed bed, the radial distribution of molar loadings, q_i , within a spherical crystallite, of radius r_c , is obtained from a solution of a set of differential equations describing the uptake

$$\frac{\partial q_i(r, t)}{\partial t} = -\frac{1}{\rho} \frac{1}{r^2} \frac{\partial}{\partial r} (r^2 N_i) \quad (3)$$

The molar flux N_i of component i is described by the simplified version of the Maxwell-Stefan equations in which both correlation effects and thermodynamic coupling effects are considered to be of negligible importance [4]

$$N_i = -\rho \mathcal{D}_i \frac{\partial q_i}{\partial r} \quad (4)$$

Summing equation (2) over all n species in the mixture allows calculation of the *total average* molar loading of the mixture within the crystallite

$$\bar{q}_t(t, z) = \sum_{i=1}^n \bar{q}_i(t, z) \quad (5)$$

The *interstitial* gas velocity is related to the *superficial* gas velocity by

$$v = \frac{u}{\varepsilon} \quad (6)$$

In industrial practice, the most common operation uses a step-wise input of mixtures to be separated into an adsorber bed that is initially free of adsorbates, i.e. we have the initial condition

$$t = 0; \quad q_i(0, z) = 0 \quad (7)$$

At time, $t = 0$, the inlet to the adsorber, $z = 0$, is subjected to a step input of the n -component gas mixture and this step input is maintained till the end of the adsorption cycle when steady-state conditions are reached.

$$t \geq 0; \quad p_i(0, t) = p_{i0}; \quad u(0, t) = u_0 \quad (8)$$

where u_0 is the superficial gas velocity at the inlet to the adsorber.

The breakthrough characteristics for any component is essentially dictated by two sets of parameters: (a) The characteristic contact time $\frac{L}{v} = \frac{L\varepsilon}{u}$ between the crystallites and the

surrounding fluid phase, and (b) $\frac{D_i}{r_c^2}$, that reflect the importance of intra-crystalline diffusion

limitations. It is common to use the dimensionless time, $\tau = \frac{tu}{L\varepsilon}$, obtained by dividing the actual

time, t , by the characteristic time, $\frac{L\varepsilon}{u}$ when plotting simulated breakthrough curves [3].

If the value of $\frac{D_i}{r_c^2}$ is large enough to ensure that intra-crystalline gradients are absent and the entire crystallite particle can be considered to be in thermodynamic equilibrium with the surrounding bulk gas phase at that time t , and position z of the adsorber

$$\bar{q}_i(t, z) = q_i(t, z) \quad (9)$$

The molar loadings at the *outer surface* of the crystallites, i.e. at $r = r_c$, are calculated on the basis of adsorption equilibrium with the bulk gas phase partial pressures p_i at that position z and time t . The adsorption equilibrium can be calculated on the basis of the IAST. The assumption of thermodynamic equilibrium at every position z , and any time t , i.e. invoking Equation (5), generally results in sharp breakthroughs for each component. Sharp breakthroughs are desirable in practice because this would result in high productivity of pure products. Essentially, the influence of intra-crystalline diffusion is to reduce the productivity of pure gases. For all the breakthrough calculations reported in this work, we assume negligible diffusion resistances for all materials and we invoke the simplified Equation (5).

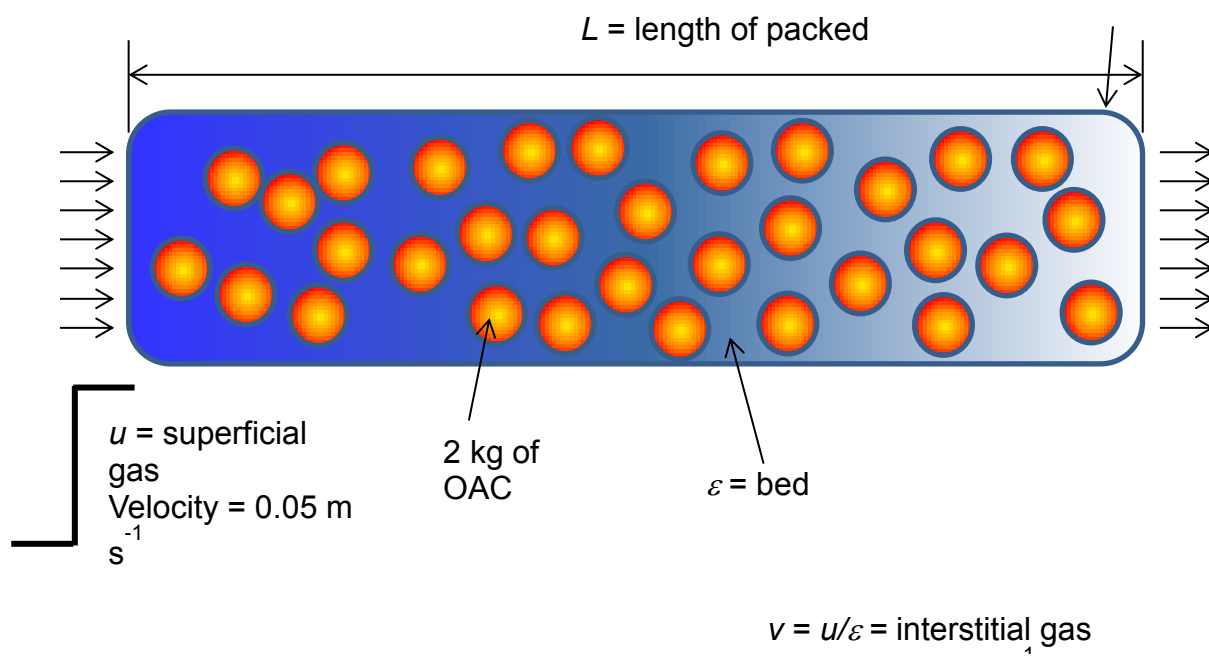


Figure S6. Schematic of the breakthrough apparatus.

Notation

b	Langmuir-Freundlich constant for species i at adsorption site A, $\text{Pa}^{-\nu_i}$
c_i	molar concentration of species i in gas mixture, mol m^{-3}
c_{i0}	molar concentration of species i in gas mixture at inlet to adsorber, mol m^{-3}
E	energy parameter, J mol^{-1}
L	length of packed bed adsorber, m
N_i	molar flux of species i , $\text{mol m}^{-2} \text{s}^{-1}$
p_i	partial pressure of species i in mixture, Pa
p_t	total system pressure, Pa
q_i	component molar loading of species i , mol kg^{-1}
$\bar{q}_i(t)$	spatially averaged component molar loading of species i , mol kg^{-1}
Q_{st}	isosteric heat of adsorption, J mol^{-1}
r_c	radius of crystallite, m
R	gas constant, $8.314 \text{ J mol}^{-1} \text{ K}^{-1}$
t	time, s
T	absolute temperature, K
u	superficial gas velocity in packed bed, m s^{-1}
v	interstitial gas velocity in packed bed, m s^{-1}

Greek letters

ε	voidage of packed bed, dimensionless
ρ	framework density, kg m^{-3}
τ	time, dimensionless

Reference

- [1]. Myers, A. L.; Prausnitz, J. M. Thermodynamics of mixed gas adsorption, A.I.Ch.E.J. 1965, 11, 121-130.
- [2]. Myers AL. Equation of state for adsorption of gases and their mixtures in porous materials. Adsorption. 2003 Mar;9(1):9-16.
- [3]. Krishna R, Long JR. Screening metal-organic frameworks by analysis of transient breakthrough of gas mixtures in a fixed bed adsorber. J Phys Chem C. 2011;115:12941-50.
- [4]. Krishna R. The Maxwell-Stefan Description of Mixture Diffusion in Nanoporous Crystalline Materials. Microporous Mesoporous Mater. 2014;185:30-50.
- [5]. Krishna R, Baur R. Modelling issues in zeolite based separation processes. Sep Purif Technol. 2003;33:213-54.